Article

J. Mex. Chem. Soc. **2019**, *63*(3)
Special Issue

ISSN-e 2594-0317

Electrocatalytic Production of Hydrogen Gas by a Cobalt Formamidinate Complex

Yanyu Wu[1], Luis M. Aguirre Quintana[1], Karen Ventura[1], Isabel Barraza Alvarez[1], Alejandro Metta-Magaña[1] and Dino Villagrán[1,*]

[1]Department of Chemistry and Biochemistry, The University of Texas at El Paso, El Paso, Texas 79968

Received September 4th, 2018; Accepted June 11th, 2019.

DOI: http://dx.doi.org/10.29356/jmcs.v63i3.535

Abstract. A molecular cobalt complex, $Co(DippF)_2$ (where DippF is the anion of N,N'-bis[2,6-diisopropylphenyl]-formamidine), (**1**), is able to electrochemically produce hydrogen gas from the reduction of organic acids in homogeneous solutions. Compound **1** has a distorted square planar structure as evidenced through X-ray crystallography studies, and an effective magnetic moment of 4.13, obtained by the Evans method, that corresponds to three unpaired electrons. Compound **1** shows an irreversible cathodic peak at –1.59 V vs Fc/Fc^+ which is assigned to the reduction of Co^{II} to Co^{I}. In the presence of organic acids the onset of catalytic current is observed at –1.2 V, –1.45 V and –1.89 V vs. Fc/Fc^+ with *p*-toluenesulfonic acid, benzoic acid and phenol as the proton source, respectively, in MeCN as the solvent. Detection of hydrogen gas was obtained by GC-MS with Faradaic efficiencies ranging from 85% to 100%. Kinetic studies using foot-of-the-wave analysis (FOWA) reveal a linear dependence of the observed rate constant, k_{obs}, against acid concentration in the range of 0.065 to 10.02 s^{-1}.
Keywords: cobalt; formamidinate; electrocatalytic; hydrogen gas.

Resumen. Un complejo molecular de cobalto, Co(DippF)2 (donde DippF es el anión de la N,N'-bis[2,6-diisopropilfenil]-formamidina), (1), es capaz de producir gas hidrógeno electroquímicamente mediante la reducción de ácidos orgánicos en soluciones homogéneas. El compuesto 1 tiene una estructura cuadrada plana distorsionada como se evidencia por estudios de cristalografía de rayos-X, y un momento magnético efectivo de 4.13, obtenido por el método de Evans, que corresponde a tres electrones no apareados. El compuesto 1 muestra un pico catódico irreversible a –1.59 V contra Fc/Fc+ que es asignado a la reducción de CoII a CoI. En la presencia de ácidos orgánicos el principio de corriente catalítica se observa a –1.2 V, –1.45 V y –1.89 V vs. Fc/Fc+ con ácido p-toluensulfónico, ácido benzoico y fenol como la fuente de protones, respectivamente, en MeCN como el solvente. La detección de gas hidrógeno fue obtenida por GC-MS con eficiencias faradaicas de 85% a 100%. Estudios cinéticos usando análisis de base de onda (FOWA por sus siglas en inglés) revelan una dependencia lineal de la constante de reacción observada, kobs, contra la concentración de ácido en el rango de 0.065 a 10.02 s-1.
Palabras clave: cobalto; formamidinato; electrocatalítico; gas hidrógeno.

Introduction

The exponential global economic and population growth has resulted in a rapid depletion of fossil fuel resources and in an increase of environmental concerns that accompany the combustion of these energy supplies.[1] Therefore exploring renewable, sustainable and clean alternative energy sources is fundamental to address these pressing issues.[1] Hydrogen gas produced through hydrogen evolution reactions (HERs) has been considered as a promising alternative fuel due to its high energy density, and its clean and carbon-free

J. Mex. Chem. Soc. **2019**, *63*(3)
Special Issue

ISSN-e 2594-0317

nature.[2-4] However, the main challenges of HERs are their high overpotential and sluggish kinetics.[5,6] Thus, to facilitate these reactions, efficient and robust catalysts are required.[7] Although platinum metal has been well demonstrated as the best HER electrocatalyst showing zero overpotential and large current density, its use is highly restricted by its high cost and scarcity.[8] In order to achieve more economically and environmentally viable hydrogen production, significant efforts have been made to explore earth-abundant materials based catalytic systems.[9,10]

Current research on HERs mainly focus on transition metal (Fe, Co, Ni, Mn) and metal-free based electrocatalysts.[9,11-17] Molecular HER electrocatalysts have received substantial interest due to their ease of rational tuning of chemical properties and redox potentials to control their catalytic performance and selectivity.[18-20] In contrast to their bulk heterogeneous counterparts, homogeneous HER molecular catalysts allow for detailed mechanistic study of hydrogen generation by utilizing spectroscopic measurements, among other techniques.[21,22] One of the most frequently studied groups of molecular electrocatalysts are cobalt-nitrogen coordinated complexes such as cobalt diglyoximes, cobalt porphyrins, cobalt salens, cobalt corroles and cobalt chlorins, etc.[23-29] Most of the cobalt complexes studied for hydrogen evolution are supported by electron-withdrawing ligands that tune the redox profile of the metal center by bringing the reduction potential to more anodic ranges, or by redox non-innocent ligands that can participate as electron reservoirs.[30-31] By contrast, cobalt-nitrogen coordinated complexes based HER electrocatalysts with electron-donating ligands are rare. Yet, the use of electron-donating ligands can potentially increase the electron-richness of the cobalt centers and, thus, enhance the reactivity at the catalytic center. Thus, further exploration of cobalt-nitrogen coordinated complexes bearing electron-donating ligands can provide new insight into the development of new ligand architectures that can improve the performance of homogeneous HER electrocatalysts.

Herein, we report the synthesis of a novel cobalt complex (**1**) where a single metal center is supported by two electron rich nitrogen-based DippF ligands (DippF = N,N'-bis[2,6-diisopropylphenyl]-formamidinate). We characterized **1** by spectroscopic means including UV-vis, nuclear magnetic resonance (NMR) spectroscopies and X-ray crystallography. Complex **1** was assessed as an electrocatalyst for hydrogen gas evolution by electrochemical measurements in MeCN with three different organic acids, namely *p*-toluenesulfonic (*tosic*) acid, benzoic acid and phenol. HER kinetic studies were also performed by foot-of-the-wave analysis (FOWA) in order to provide insights of the relationship between rate constant and acid concentration.

Experimental

General considerations

Synthesis of **1** was accomplished using standard Schlenk techniques under N_2 atmosphere and a dry N_2-filled glovebox. All solvents used were dried using a Pure Process Technology solvent purification system.

Materials

All materials used were purchased from commercially available sources. Tetrabutylammonium hexafluorophosphate ($TBAPF_6$), *p*-toluenesulfonic (*tosic*) acid, benzoic acid, phenol and $CoCl_2 \cdot 6H_2O$ were dried under vacuum at 60 °C prior to use. The remaining chemicals were used as received. HDippF was synthesized according to a previously reported method.[32]

Physical measurements

^{1}H NMR spectroscopy was recorded on a Bruker 400 MHz NMR spectrometer, using deuterated benzene (C_6D_6) as the solvent. The residual protic signal of C_6D_6 was used as the internal standard (δ=7.16 ppm). UV-vis spectra were obtained using a SEC2000 instrument with a VISUAL SPECTRA 2.1 software.

Information of X-ray crystal structure of 1

A specimen of **1** was used for the X-ray crystallographic analysis. The X-ray intensity data were measured on a Bruker SMART APEX CCD system equipped with a graphite monochromator and a MoKα fine-

J. Mex. Chem. Soc. **2019**, *63*(3)
Special Issue

ISSN-e 2594-0317

focus tube (λ = 0.71073 Å).The total exposure time was 4.00 hours. The frames were integrated with the Bruker SAINT software package using a narrow-frame algorithm. The integration of the data using an orthorhombic unit cell yielded a total of 22716 reflections to a maximum θ angle of 26.00° (0.81 Å resolution), of which 4567 were independent (average redundancy 4.974, completeness = 100.0%, Rint = 3.81%, Rsig = 3.65%) and 4362 (95.51%) were greater than 2σ(F2). The final cell constants of a = 14.4164(7) Å, b = 20.1178(10) Å, c = 15.9876(8) Å, volume = 4636.8(4) Å3, are based upon the refinement of the XYZ-centroids of 9910 reflections above 20 σ(I) with 4.784° < 2θ < 57.66°. Data were corrected for absorption effects using the multi-scan method (SADABS). The ratio of minimum to maximum apparent transmission was 0.889.

The structure was solved and refined using the Bruker SHELXTL Software Package, using the space group C 2 2 21, with Z = 4 for the formula unit, $C_{50}H_{68}CoN4$. The final anisotropic full-matrix least-squares refinement on F2 with 278 variables converged at R1 = 5.46%, for the observed data and wR2 = 15.32% for all data. The goodness-of-fit was 1.088. The largest peak in the final difference electron density synthesis was 0.486 e-/Å3 and the largest hole was -0.612 e-/Å3 with an RMS deviation of 0.079 e-/Å3. On the basis of the final model, the calculated density was 1.123 g/cm3 and F(000), 1692 e-.

Table 1. Data collection and structure refinement for **1**.

Diffractometer	Bruker SMART APEX CCD	
Radiation source	fine-focus tube, MoKα	
Theta range for data collection	1.74 to 26.00°	
Index ranges	-17<=h<=11, -24<=k<=24, -19<=l<=19	
Reflections collected	22716	
Independent reflections	4567 [R(int) = 0.0381]	
Coverage of independent reflections	100.0%	
Absorption correction	multi-scan	
Structure solution technique	direct methods	
Structure solution program	SHELXS-97(Sheldrick 2008)	
Refinement method	Full-matrix least-squares on F^2	
Refinement program	SHELXL-2014/6 (Sheldrick, 2014)	
Function minimized	$\Sigma w(F_o^2 - F_c^2)^2$	
Data / restraints / parameters	4567 / 43 / 278	
Goodness-of-fit on F^2	1.088	
Final R indices	4362 data; I>2σ(I)	R1 = 0.0546, wR2 = 0.1517
	all data	R1 = 0.0566, wR2 = 0.1532
Weighting scheme	$w=1/[\sigma^2(F_o^2)+(0.0881P)^2+7.7217P]$ where $P=(F_o^2+2F_c^2)/3$	
Absolute structure parameter	0.0(0)	
Largest diff. peak and hole	0.486 and -0.612 eÅ^{-3}	
R.M.S. deviation from mean	0.079 eÅ^{-3}	

Evans method

The magnetic susceptibility was measured through ^{1}H NMR spectroscopy, which was carried out with a sealed capillary tube containing pure C_6D_6 placed inside an NMR tube already loaded with a solution of **1** (0.0160 g) in C_6D_6 (1.5 mL) in order to measure the chemical shift difference of the solvent caused by the different electronic environments. The number of unpaired electrons (*n*) was calculated as shown below:[33,34]

J. Mex. Chem. Soc. **2019**, *63*(3)
Special Issue

ISSN-e 2594-0317

$$\chi_{mass} = \frac{3\Delta f}{4\pi f m} + \chi_0 + \frac{\chi_0(d_0 - d_s)}{m} \quad \text{(Eq.1)}$$

where, χ_{mass} is the mass susceptibility, Δf is the frequency separation, f is the NMR frequency being studied ($400*10^6$ Hz), m is the mass concentration (g/cm^3) of **1**, χ_0 is the mass susceptibility of the solvent ($–8.8*10^{-9}$ m^3/kg for benzene), d_o is the density of the solvent and d_s is the density of the solution.

The molar susceptibility (χ_M) is given by:

$$\chi_M = \mathrm{M}\chi_{mass} \quad \text{(Eq.2)}$$

$$\chi_M = N_0\mu_0\xi + \chi_M^{para} \quad \text{(Eq.3)}$$

$$\chi_M^{para} = \chi_M - N_0\mu_0\xi \quad \text{(Eq.4)}$$

where, N_0 is the Avogadro's number, μ_0 is the vacuum permeability ($4\pi*10^{-7}$ NA^{-2}), ξ is magnetizability, $N_0\mu_0\xi$ is the diamagnetic contribution and χ_M^{para} is the paramagnetic contribution. The effective paramagnetic moment is expressed as:

$$\mu_{eff} = 797.8\sqrt{T\chi_M^{para}}\ \ Bohr\ Magneton \quad \text{(Eq.5)}$$

The number of unpaired electrons (n) can be finally calculated through:

$$\mu_{eff}(spin\ only) = \sqrt{n(n+2)} \quad \text{(Eq.6)}$$

Synthesis of 1

Synthesis of **1** was performed in a dried N_2-filled glovebox. Anhydrous $CoCl_2$ (0.500 g, 3.85 mmol) was dissolved in 20 mL THF using a 50 mL round-bottom flask. Then, HDippF (2.80 g, 7.70 mmol) was added to the solution. Subsequently, methyllithium (4.81 mL, 7.70 mmol) was added using a glass syringe. The solution changed from a sky blue to a dark aqua-green color. The resulting solution was allowed to vigorously stir under room temperature for three hours. Afterwards, diethyl ether (Et_2O) was added to precipitate the LiCl byproduct. The resulting suspension was filtered using a medium coarse glass frit packed with Celite. The filtrate was dried under reduced pressure to obtain 1.058 g of the final green product. The product was crystallized using of a concentrated solution of Et_2O. Yield 35.05%. UV-vis: λ max: 564, 628, and 674 nm.

J. Mex. Chem. Soc. **2019**, *63*(3)
Special Issue

ISSN-e 2594-0317

Electrochemical measurements

Electrochemical measurements were recorded on a CHI760D potentiostat using a three-electrode electrochemical cell in a dry N_2-filled glovebox, with glassy carbon (4 mm diameter) as the working electrode, platinum wire and Ag/Ag^+ as the counter and reference electrode, respectively. Ferrocene (Fc) was added subsequently after each measurement as an internal reference and all potentials displayed are referred to ferrocene/ferrocenium (Fc/Fc^+) redox couple.

Hydrogen gas detection

Hydrogen gas was confirmed and quantified using a Gas Chromatograph (GC) after performing bulk electrolysis. Bulk electrolysis was operated using a sealed custom-built three-electrode electrochemical cell with an H shape. The working electrode (1 cm^2 carbon rod), reference electrode (Ag/Ag^+) were separated with the counter electrode (Pt mesh) through a glass frit. Solutions containing 50 mL of 1 mM of **1**, 0.1 M of $TBAPF_6$ and 10 mM of the respective acid studied (*tosic* acid, benzoic acid, phenol) in MeCN were used for bulk electrolysis at a constant potential of –2.0 V vs. Fc/Fc^+ for an hour. An aliquot of 300 µL of the gas in the headspace in the side of the cell containing the working electrode was injected to the GC for analysis.

Calculation of k_{obs} and k_{cat} from foot-of-the-wave analysis (FOWA)

The HER kinetics can be measured by the foot-of-the-wave analysis (FOWA), which has been developed by Savéant and coworkers.[35] For an ECEC or ECCE mechanistic process,[35-36] the current is described by:

$$i = \frac{2\mathrm{FA}C_p^0\sqrt{\mathrm{D}k_{obs}}}{1 + e^{\left[\frac{F}{RT}(E - E_{cat/2})\right]}} \quad \text{(Eq. 7)}$$

where, F is the Faraday constant (96485 C/mol), A is the surface area of the working electrode (cm^2), C_p^0 is the concentration of the catalyst (mol/L), D is the diffusion coefficient (cm^2/s) and k_{obs} is the observed rate constant.

According to the Randles-Sevcik equation, the peak current is:[37]

$$i_p = 0.4463\ \mathrm{FA}C_{\mathrm{p}}^0\sqrt{\frac{\mathrm{F}\nu\mathrm{D}}{\mathrm{RT}}} \quad \text{(Eq. 8)}$$

where, ν is the scan rate.

By diving Eq.7 with Eq.8, we can get:

$$\frac{i}{i_p} = \frac{2\sqrt{\frac{\mathrm{RT}}{\mathrm{F}\nu}}\sqrt{k_{obs}}}{0.4463} * \frac{1}{1 + e^{\left[\frac{\mathrm{F}}{\mathrm{RT}}(\mathrm{E} - \mathrm{E}_{\mathrm{cat}/2})\right]}} \quad \text{(Eq. 9)}$$

J. Mex. Chem. Soc. **2019**, *63*(3)
Special Issue

ISSN-e 2594-0317

After plotting $\frac{i}{i_p}$ versus $\frac{1}{1+e^{\left[\frac{F}{RT}\left(E-E_{cat/2}\right)\right]}}$ from the linear region we can obtain a slope of m, which

$$m = \frac{2\sqrt{\frac{RT}{Fv}}\sqrt{k_{obs}}}{0.4463} \quad \text{(Eq. 10)}$$

Thus k_{obs} can be obtained from

$$k_{obs} = \frac{(m)^2(0.4463)^2\, Fv}{4RT} \quad \text{(Eq. 11)}$$

Then the catalytic rate constant (k_{cat}) is calculated from:

$$k_{cat} = \frac{k_{obs}}{[H^+]} \quad \text{(Eq. 12)}$$

Calculation of structural geometry index τ_4 for a mononuclear 4-coordinate complex

To disambiguate whether **1** bears closer structural resemblance to a square planar or tetrahedral complex, the model proposed by Yang et al. (Eq. 13) was used.[38] In this equation, where τ_4 is the structural index, β and α are the two largest valence angles in a 4-coordinate molecule respectively, and θ is 109.5°. For a 4-coordinate species, a τ_4 of 1 represents a tetrahedral molecule while a τ_4 of 0 indicates a square planar molecule.

$$\tau_4 = \frac{360 - (\beta + \alpha)}{360 - 2\theta} \quad \text{(Eq. 13)}$$

J. Mex. Chem. Soc. **2019**, *63*(3)
Special Issue

ISSN-e 2594-0317

Results and discussion

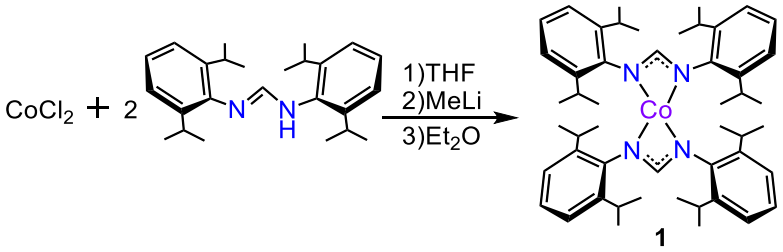

Scheme 1. Synthetic scheme of 1.

The solid-state structure of **1** was confirmed by X-ray crystallography (Fig. 1) and the detailed crystallographic data are summarized in Table 2. The bond distances of Co(1)-N(1) and Co(1)-N(2) are 1.998(3) Å and 1.999(3) Å, respectively, which are longer than those of the reported Co diglyoxime complex (1.886(5) Å).[23] The N2-Co1-N2, N1-Co1-N1, N2-Co1-N1 bond angles are found to be 155.0º (2), 151.0º (2), and 119.66º (14) respectively. Based on the bond angles, the calculated geometry index τ_4 is 0.38. Thus, **1** is assigned as a distorted square planar complex.

Table 2. Sample and crystal data for **1**.

Identification code	$Co(DippF)_2$	
Chemical formula	$C_{50}H_{68}CoN_4$	
Formula weight	784.01 g/mol	
Temperature	100(2) K	
Wavelength	0.71073 Å	
Crystal system	orthorhombic	
Space group	C 2 2 21	
Unit cell dimensions	a = 14.4164(7) Å	α = 90°
	b = 20.1178(10) Å	β = 90°
	c = 15.9876(8) Å	γ = 90°
Volume	4636.8(4) $Å^3$	
Z	4	
Density (calculated)	1.123 g/cm^3	
Absorption coefficient	0.406 mm^{-1}	
F(000)	1692	

J. Mex. Chem. Soc. **2019**, *63*(3)
Special Issue

ISSN-e 2594-0317

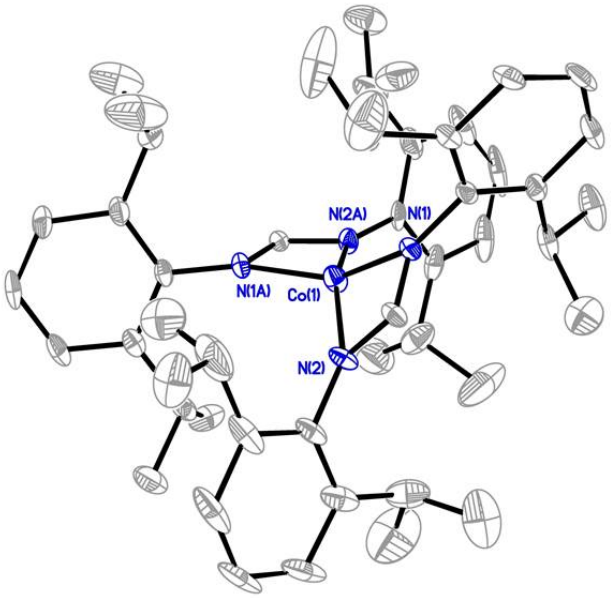

Fig. 1. Solid-state crystal structure of **1** with thermal ellipsoid shown to be 50%. Hydrogen atoms were omitted for clarity. R(int)= 8.58%, R(sigma)= 2.95%.

Characterization of **1** by ^{1}H NMR proved challenging due to the intense paramagnetic broadening of the observed signals, reflecting the paramagnetic nature of the complex, and consistent with previous reports of 4-coordinate d^7 Co(II) complexes.[39,40] The magnetic susceptibility of **1** was probed through the Evans method. The ^{1}H NMR signal for benzene is shifted by +0.51 ppm in the presence of **1**, resulting in a μ_{eff} of 4.13 corresponding to three unpaired electrons (*vide supra*). This is consistent with other 4-coordinate cobalt complexes bearing nitrogen-donor ligands.[41] The higher μ_{eff} value compared to the predicted spin-only μ_{eff} of 3.87 is attributed to the typical spin-orbit coupling experienced by cobalt.[42,43]

Cyclic voltammograms (CVs) of **1** are presented in Figures 2-4. Compound **1** shows one nonreversible one-electron reduction wave at E_p = –1.59 V vs. Fc/Fc$^+$, resulting from the Co^{II}/Co^{I} reduction couple. The nonreversibility of this event can be attributed to the electron-rich nature of **1**. Upon addition of *tosic* acid (pK$_a$= 8.5 in MeCN), a catalytic wave is observed with an onset potential of –1.2 V vs. Fc/Fc$^+$, accompanying with another reduction wave at E_p = –1.73 V vs. Fc/Fc$^+$. Another two significantly less acidic proton sources, namely benzoic acid (pK$_a$= 21.51 in MeCN) and phenol (pK$_a$= 29.14 in MeCN), were also introduced to evaluate the electrocatalytic activity of **1**. The CVs of **1** upon addition of both benzoic acid and phenol show considerable increase of cathodic catalytic current for proton reduction, with an onset potential of –1.45 V and –1.89 V vs. Fc/Fc$^+$ for benzoic acid and phenol, respectively (Figures 3-4). The ability of **1** to catalyze proton reduction in weak acidic media, which is noteworthy for this type of study, can be attributed to the enhanced electro-activity of the cobalt center due to the electron-donating formamidinate ligand. Hydrogen gas detection and quantification were carried out after performing bulk electrolysis for an hour at a constant potential of –2.0 V vs. Fc/Fc$^+$ using 1 mM of **1** and 10 mM of the chosen acids. The accumulated charge over time (Fig. 5) shows 36.16, 14.26, 8.08 C of the passed charge for an hour of electrolysis when using *tosic* acid, benzoic acid and phenol, respectively, corresponding to Faradaic efficiencies of 91.4%, 85.0% and 100% for hydrogen production.

J. Mex. Chem. Soc. **2019**, *63*(3)
Special Issue

ISSN-e 2594-0317

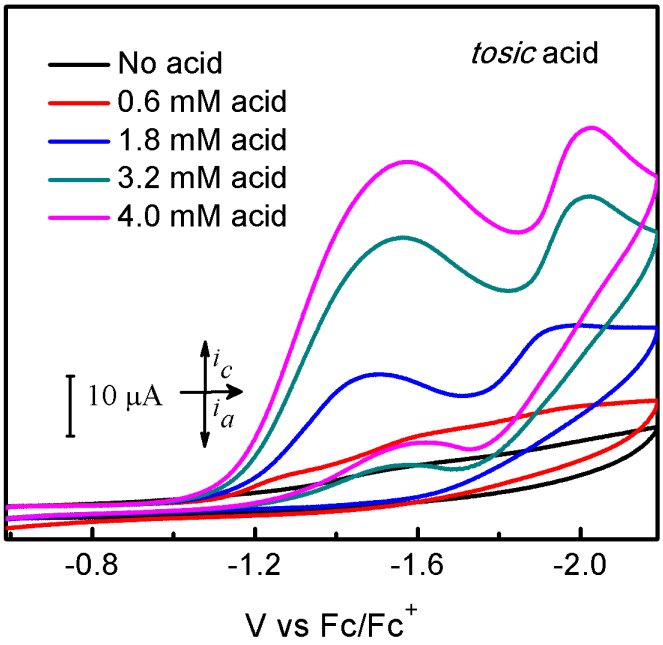

Fig. 2. Cyclic voltammograms of 1 mM **1** without acid (black line) and with *tosic* acid (colored lines) in MeCN solution containing 0.1 M $TBAPF_6$. Scan rate: 100 mV/s; glassy carbon electrode (4 mm diameter).

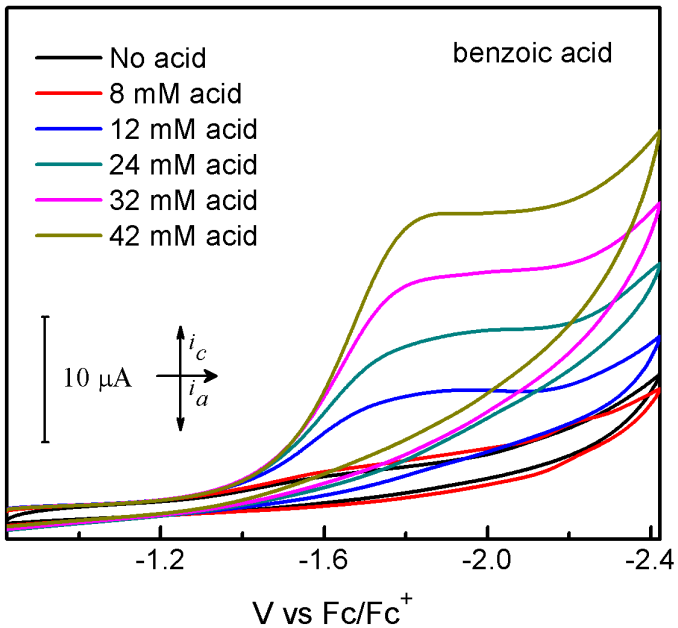

Fig. 3. Cyclic voltammograms of 1 mM **1** without acid (black line) and with benzoic acid (colored lines) in MeCN solution containing 0.1 M $TBAPF_6$. Scan rate: 100 mV/s; glassy carbon electrode (4 mm diameter).

J. Mex. Chem. Soc. **2019**, *63*(3)
Special Issue

ISSN-e 2594-0317

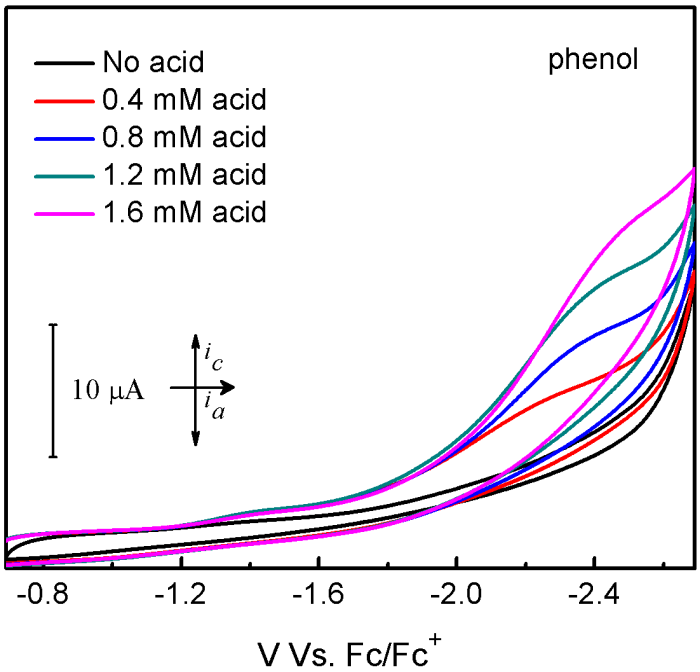

Fig. 4. Cyclic voltammograms of 1 mM **1** without acid (black line) and with phenol (colored lines) in MeCN solution containing 0.1 M $TBAPF_6$. Scan rate: 100 mV/s; glassy carbon electrode (4 mm diameter).

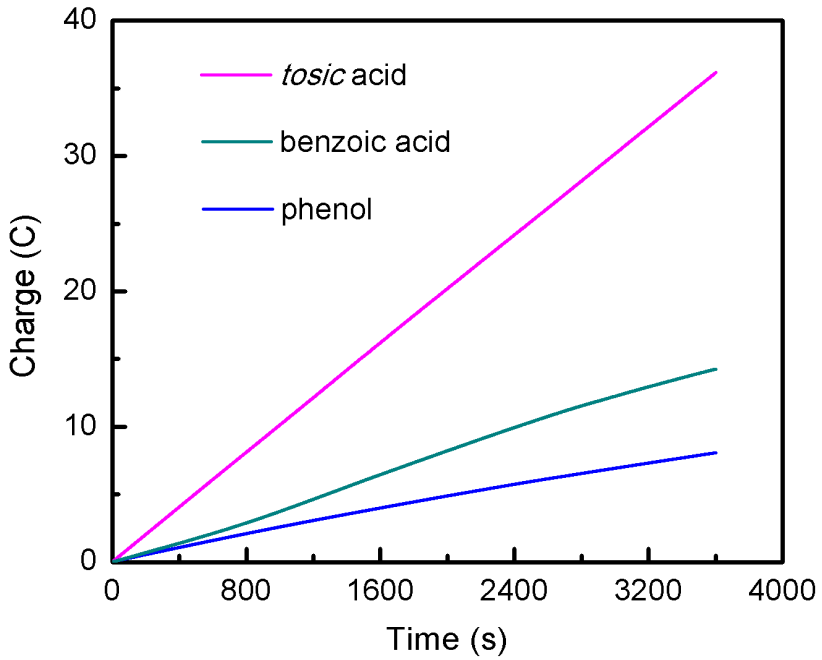

Fig. 5. Bulk electrolysis experiments of 1 mM **1** containing 10 mM of *tosic* acid, benzoic acid and phenol, respectively. Applied potential: – 2.0 V vs. Fc/Fc^+.

J. Mex. Chem. Soc. **2019**, *63*(3)
Special Issue

ISSN-e 2594-0317

The reaction kinetics of HER using **1** with *tosic* acid was studied through the use of foot-of-the-wave analysis (FOWA). The FOWA plot is presented in Fig. 6 **(a)**, which is derived from the linear sweep voltammograms shown in Fig. 6 **(b)**. The observed rate constants (k_{obs}) and catalytic rate constants (k_{cat}) at different concentrations of acid addition are summarized in Table 3 (see experimental section for detailed calculation). The relationship of k_{obs} with acid concentration is linear (Fig. 7), suggesting there is a first order dependence on acid concentration.

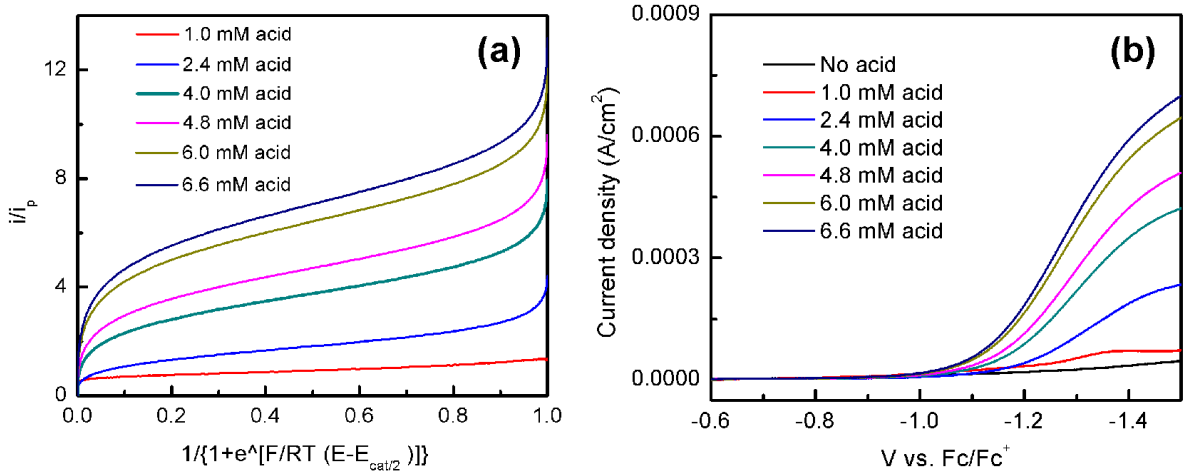

Fig. 6. (a) FOWA plots of 1 mM of **1** at different concentration of *tosic* acid. Scan rate: 100 mV/s; **(b)** Linear sweep voltammograms of **1** in MeCN with 0.1 M $TBAPF_6$ titration with *tosic* acid.

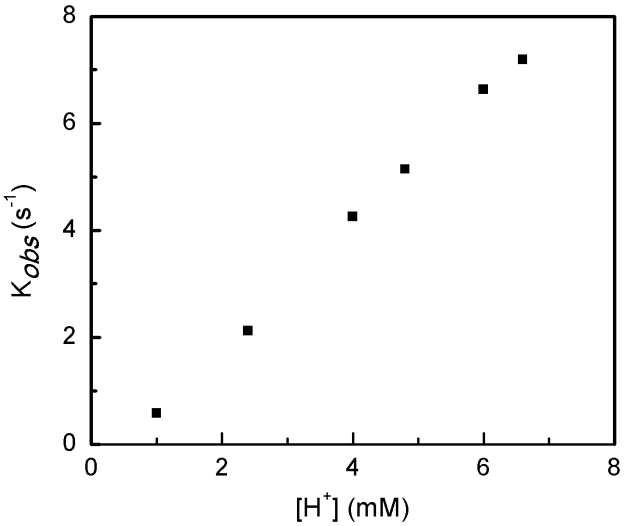

Fig. 7. Plots of observed rate constant (k_{obs}) versus acid concentration ($[H^+]$).

J. Mex. Chem. Soc. **2019**, *63*(3)
Special Issue

ISSN-e 2594-0317

Table 3. Summary of the results of FOWA slope (*m*), k_{obs} and k_{cat} at different acid concentration.

$[H^+]$ (mM)	M	k_{obs} (s^{-1})	k_{cat} ($M^{-1}s^{-1}$)
1.0	0.58	0.0652	65.2
2.4	2.12	0.872	363
4.0	4.25	3.50	875
4.8	5.14	5.12	1066
6.0	6.63	8.52	1420
6.6	7.19	10.02	1518

Conclusion

In conclusion, we have successfully synthesized a cobalt complex anchored by formamidinate ligand. Structural analysis by X-ray crystallography shows that **1** has a distorted square planar chemical structure and magnetic susceptibility measurements show a μ_{eff} of 4.13 B.M. at room temperature, indicative of an electronic structure bearing three unpaired electrons. This molecule is found to be active for electrochemical hydrogen generation with both strong acid and weak acid substrates in MeCN. The electrochemical onset potentials for hydrogen generation range from –1.2 V to –1.89 V vs. Fc/Fc^+. This work shows the potential of using electron rich ligand architectures for tuning the redox activity of cobalt HER electrocatalysts.

Acknowledgment

This work was financially supported by NSF under award number CHE-1305124. LMAQ thanks COURI-Meritus at UTEP and CCI-Solar for research finance. IBA thanks MARC for an undergraduate scholarship.

References

1. Gray, H. B. *Nat. Chem.* **2009**, *1* (1), 7–7.
2. Cook, T. R.; Dogutan, D. K.; Reece, S. Y.; Surendranath, Y.; Teets, T. S.; Nocera, D. G. *Chem. Rev.* **2010**, *110* (11), 6474–6502.
3. Lewis, N. S.; Nocera, D. G. *Proc. Natl. Acad. Sci.* **2006**, *103* (43), 15729–15735.
4. Sanchez, J.; Ramos-Garcés, M. V.; Narkeviciute, I.; Colón, J. L.; Jaramillo, T. F. *Catalysts* **2017**, *7* (5), 132.
5. Wang Lihuan; Tranca Diana C.; Zhang Jian; Qi Yanpeng; Sfaelou Stavroula; Zhang Tao; Dong Renhao; Zhuang Xiaodong; Zheng Zhikun; Seifert Gotthard. *Small* **2017**, *13* (37), 1700783.
6. Turner, J. A. *Science* **2004**, *305* (5686), 972–974.
7. Thoi, V. S.; Sun, Y.; Long, J. R.; Chang, C. J. *Chem. Soc. Rev.* **2013**, *42* (6), 2388–2400.

J. Mex. Chem. Soc. **2019**, *63*(3)
Special Issue

ISSN-e 2594-0317

8. Popczun, E. J.; Read, C. G.; Roske, C. W.; Lewis, N. S.; Schaak, R. E. *Angew. Chem. Int. Ed Engl.* **2014**, *53* (21), 5427–5430.
9. Wang, M.; Chen, L.; Sun, L. *Energy Environ. Sci.* **2012**, *5* (5), 6763–6778.
10. Faber, M. S.; Lukowski, M. A.; Ding, Q.; Kaiser, N. S.; Jin, S. *J. Phys. Chem. C* **2014**, *118* (37), 21347–21356.
11. 11. Chen, X.; Wang, D.; Wang, Z.; Zhou, P.; Wu, Z.; Jiang, F. *Chem. Commun.* **2014**, *50* (79), 11683–11685.
12. 12. Bediako, D. K.; Solis, B. H.; Dogutan, D. K.; Roubelakis, M. M.; Maher, A. G.; Lee, C. H.; Chambers, M. B.; Hammes-Schiffer, S.; Nocera, D. G. *Proc. Natl. Acad. Sci. U. S. A.* **2014**, *111* (42), 15001–15006.
13. 13. Bayati, M. *Chemcatchem* **2017**, *9*.
14. 14. Patra, B. C.; Khilari, S.; Manna, R. N.; Mondal, S.; Pradhan, D.; Pradhan, A.; Bhaumik, A. *ACS Catal.* **2017**, *7* (9), 6120–6127.
15. 15. Yap, C. P.; Poh, H. T.; Fan, W. Y. *RSC Adv.* **2016**, *6* (7), 5903–5906.
16. 16. Zheng, Y.; Jiao, Y.; Zhu, Y.; Li, L. H.; Han, Y.; Chen, Y.; Du, A.; Jaroniec, M.; Qiao, S. Z. *Nat. Commun.* **2014**, *5*, ncomms4783.
17. 17. Wu, Y.; Zarei-Chaleshtori, M.; Torres, B.; Akter, T.; Diaz-Moreno, C.; Saupe, G. B.; Lopez, J. A.; Chianelli, R. R.; Villagrán, D. *Int. J. Hydrog. Energy* **2017**, *42* (32), 20669–20676.
18. 18. Solis, B. H.; Hammes-Schiffer, S. *J. Am. Chem. Soc.* **2011**, *133* (47), 19036–19039.
19. 19. Matson, B. D.; Peters, J. C. *ACS Catal.* **2018**, *8* (2), 1448–1455.
20. 20. McCrory, C. C. L.; Uyeda, C.; Peters, J. C. *J. Am. Chem. Soc.* **2012**, *134* (6), 3164–3170.
21. 21. Marinescu, S. C.; Winkler, J. R.; Gray, H. B.*Proc. Natl. Acad. Sci.* **2012**, *109* (38), 15127–15131.
22. 22. Solis, B. H.; Maher, A. G.; Dogutan, D. K.; Nocera, D. G.; Hammes-Schiffer, S. *Proc. Natl. Acad. Sci.* **2016**, *113* (3), 485–492.
23. 23. Hu, X.; Brunschwig, B. S.; Peters, J. C. *J. Am. Chem. Soc.* **2007**, *129* (29), 8988–8998.
24. 24. Bhugun, I.; Lexa, D.; Savéant, J.-M.*J. Am. Chem. Soc.* **1996**, *118* (16), 3982–3983.
25. 25. Lee, C. H.; Dogutan, D. K.; Nocera, D. G. *J. Am. Chem. Soc.* **2011**, *133* (23), 8775–8777.
26. 26. Kaeffer, N.; Chavarot-Kerlidou, M.; Artero, V. *Acc. Chem. Res.* **2015**, *48* (5), 1286–1295.
27. 27. Mondal, B.; Sengupta, K.; Rana, A.; Mahammed, A.; Botoshansky, M.; Dey, S. G.; Gross, Z.; Dey, *Inorg. Chem.* **2013**, *52* (6), 3381–3387.
28. 28. Beyene, B. B.; Mane, S. B.; Hung, C.-H. *Chem. Commun.* **2015**, *51* (81), 15067–15070.
29. 29. Fihri, A.; Artero, V.; Razavet, M.; Baffert, C.; Leibl, W.; Fontecave, M. *Angew. Chem. Int. Ed Engl.* **2008**, *47* (3), 564–567.
30. 30. Jurss, J. W.; Khnayzer, R. S.; Panetier, J. A.; Roz, K. A. E.; Nichols, E. M.; Head-Gordon, M.; Long, J. R.; Castellano, F. N.; Chang, C. J. *Chem. Sci.* **2015**, *6* (8), 4954–4972.
31. 31. Chen, L.; Khadivi, A.; Singh, M.; Jurss, J. W. *Inorg. Chem. Front.* **2017**, *4* (10), 1649–1653.
32. 32. Elkin, T.; Kulkarni, N. V.; Tumanskii, B.; Botoshansky, M.; Shimon, L. J. W.; Eisen, M. S. *Organometallics* **2013**, *32* (21), 6337–6352.
33. 33. Evans, D. F. 400.*J. Chem. Soc. Resumed* **1959**, *0* (0), 2003–2005.
34. 34. Ostfeld, D.; Cohen, I. A. *J. Chem. Educ.* **1972**, *49* (12), 829.
35. 35. Costentin, C.; Drouet, S.; Robert, M.; Savéant, J.-M. *J. Am. Chem. Soc.* **2012**, *134* (27), 11235–11242.
36. 36. Rountree, E. S.; McCarthy, B. D.; Eisenhart, T. T.; Dempsey, J. L. *Inorg. Chem.* **2014**, *53* (19), 9983–10002.
37. 37. Rountree, E. S.; Martin, D. J.; McCarthy, B. D.; Dempsey, J. L. *ACS Catal.* **2016**, *6* (5), 3326–3335.

J. Mex. Chem. Soc. **2019**, *63*(3)
Special Issue

ISSN-e 2594-0317

38. 38. Yang, L.; Powell, D. R.; Houser, R. P. *Dalton Trans. Camb. Engl. 2003* **2007**, No. 9, 955–964.
39. 39. Maher, A. G.; Passard, G.; Dogutan, D. K.; Halbach, R. L.; Anderson, B. L.; Gagliardi, C. J.; Taniguchi, M.; Lindsey, J. S.; Nocera, D. G. *ACS Catal.* **2017**, *7* (5), 3597–3606.
40. 40. Fryzuk, M. D.; Leznoff, D. B.; Thompson, R. C.; Rettig, S. J. *J. Am. Chem. Soc.* **1998**, *120* (39), 10126–10135.
41. 41. Carabineiro, S. A.; Silva, L. C.; Gomes, P. T.; Pereira, L. C. J.; Veiros, L. F.; Pascu, S. I.; Duarte, M. T.; Namorado, S.; Henriques, R. T. *Inorg. Chem.* **2007**, *46* (17), 6880–6890.
42. 42. Fink, K.; Wang, C.; Staemmler, V. *Inorg. Chem.* **1999**, *38* (17), 3847–3856.
43. 43. Gerloch, M.; Quested, P. N. *J. Chem. Soc. Inorg. Phys. Theor.* **1971**, *0* (0), 3729–3741.